

This is the accepted manuscript made available via CHORUS. The article has been published as:

## Synchronization of spin torque nano-oscillators

James Turtle, Pietro-Luciano Buono, Antonio Palacios, Christine Dabrowski, Visarath In,  
and Patrick Longhini

Phys. Rev. B **95**, 144412 — Published 12 April 2017

DOI: [10.1103/PhysRevB.95.144412](https://doi.org/10.1103/PhysRevB.95.144412)

# On The Synchronization Phenomenon of Spin Torque Nano-oscillators

James Turtle<sup>1,\*</sup>, Pietro-Luciano Buono<sup>2,†</sup>, Antonio Palacios<sup>1,‡</sup>,  
Christine Dabrowski<sup>2,§</sup>, Visarath In<sup>3,¶</sup> and Patrick Longhini<sup>3,\*\*</sup>

<sup>1</sup> *Nonlinear Dynamical Systems Group, Department of Mathematics,  
San Diego State University, San Diego, CA 92182, USA.*

<sup>2</sup> *Faculty of Science, University of Ontario Institute of Technology,  
2000 Simcoe St N, Oshawa, ON L1H 7K4, CANADA*

<sup>3</sup> *Space and Naval Warfare Systems Center Pacific, Code 71730,  
53560 Hull Street, San Diego, CA 92152-5001, USA.*

Synchronization of Spin Torque Nano-Oscillators has been a subject of extensive research as various groups try to harness the collective power of STNOs to produce a strong enough microwave signal at the nanoscale. Achieving synchronization has proven to be, however, rather difficult for even small arrays while in larger ones the task of synchronization has eluded theorist and experimentalists altogether. In this work we solve the synchronization problem, analytically and computationally, for networks of STNOs connected in series. The procedure is valid for networks of arbitrary size and it is readily extendable to other network topologies. These results should help guide future experiments and, eventually, lead to the design and fabrication of a nanoscale microwave signal generator.

PACS numbers: 74.81.Fa, 85.25.Dq, 43.25.-x, 85.25.-j

## I. INTRODUCTION

The synchronization phenomenon of Spin Torque Nano-Oscillators (STNO) has been the subject of extensive research for many years due to the potential of networks of STNOs to generate microwave signals at the nanoscale<sup>1-3</sup>. In the last few years, Adler<sup>4</sup> type injection locking has emerged as the most promising method to achieve synchronization, either through an external microwave current<sup>5-7</sup> or through a microwave magnetic field<sup>8,9</sup>. In particular, it has been shown recently, that a record number of five nano-contact STNOs<sup>10</sup> can synchronize via spin wave beams<sup>11</sup>. Non-Adlerian approaches to synchronization of nanopillar STNOs have also been considered. In Georges *et al.*<sup>12</sup>, the critical coupling strength and minimum number of STNOs for the onset of synchronization were found analytically by describing the STNOs as phase oscillators in the framework of Kuramoto<sup>13</sup>. Later, Iacocca and Akerman<sup>15</sup> provided conditions for the onset of phase instability that may be caused, surprisingly, by strong coupling in identical STNOs. It is well known, however, that amplitude can affect synchronization, specially near the onset of a Hopf bifurcation<sup>16</sup>. In fact, in STNOs amplitude and phase are intrinsically coupled by the dependence of the effective field on the magnetization<sup>17</sup>. Thus, if the Hopf bifurcation parameter is of the same scale as the coupling parameter then the amplitude is no longer negligible and the Kuramoto model reduction is no longer valid. Furthermore, when the amplitude dynamics are not negligible and the natural oscillation frequencies are not homogeneous, synchronization may be enhanced regardless of the topology of the network<sup>18</sup>. Consequently, a complete understanding of synchronization of nanopillar based STNOs, via non-Adlerian type, requires an analysis that incorporates the amplitude dynamics.

In 2005, back-to-back publications in Nature Letters

(Kaka<sup>2</sup>, a collaboration between NIST and Hitachi GST and Mancoff<sup>19</sup> from Freescale Semiconductor) showed that two STNOs tend to phase lock when they are in close proximity of one another. The coupling in these cases resulted from spin waves propagating through the continuous free layers, leading to phase locking. Soon after, Grollier *et al.*<sup>1</sup> investigated computationally the behavior of a 1D series array of  $N = 10$  electrically coupled STNOs. Their study showed that the AC current produced by each individual oscillator leads to feedback between the STNOs causing them to synchronize and that, collectively, the microwave power output of the array increases as  $N^2$ . In a follow-up study, Persson *et al.*<sup>3</sup> mapped out numerically the region of synchronization of the 1D serially connected array considered by Grollier *et al.* for the special case of  $N = 2$  STNOs. Their work shows that the region of parameter space where synchronization exists is rather small, thus explaining the difficulty (already observed by experimentalists) to achieve synchronization. Li *et al.*<sup>20</sup> showed that this difficulty was due, mainly, to the coexistence of multiple stable attractors, suggesting that the synchronization regime is highly sensitive to initial conditions. Persson *et al.*<sup>3</sup> also investigate numerically the effect of including a time-delay between the magnetization induced change in voltage and the current variation. They highlight that this increases significantly the parameter region of synchronization, especially with respect to differences in anisotropy fields between the STNOs. We determine numerically that the synchronization for 1000 STNOs is robust to non-homogeneities in the anisotropy field on the order of 4-5%, as Persson *et al.* also observes in the absence of delay. It will be worthwhile to investigate in future work the effects of time-delay and to find out whether the synchronization is robust to larger anisotropy in the network.

On a single STNO, see Fig. 1(a), an originally unpolarized electric current  $I$ , in units of Amp, is applied to the

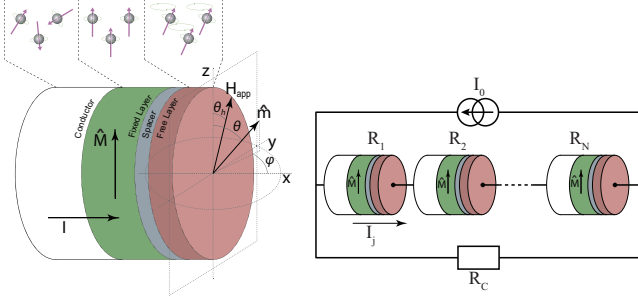


FIG. 1: (Left) Schematic representation of a nanopillar STNO. A *spin-polarized* current can exert a torque on the magnetization of the free layer and lead to steady precession. (Right) a circuit array of STNOs connected in series.

fixed magnetic layer whose magnetization is represented by  $\hat{M}$ . As the electrons pass through the layer, their spins become aligned to that of the fixed layer, thus creating a *spin-polarized* current. Then the polarized current exerts a torque on the magnetization of the free layer, which can lead to steady precession. We consider a circuit array of  $N$  identical STNOs coupled in series, see Fig. 1(b), and study the conditions to synchronize the individual precessions. Our approach employs the DC current,  $I_{DC}$ , flowing in each STNO and the angle  $\theta_h$  of the applied magnetic field as the bifurcation parameters. No injection of AC current is required. The all-to-all coupling of the network of identical STNOs implies a complete permutation symmetry which we exploit using equivariant bifurcation theory<sup>21</sup>.

We search for fully synchronized periodic oscillations in the network of  $N$  STNOs, first by finding implicit analytical expressions for Hopf bifurcation curves, in  $(I_{DC}, \theta_h)$  space, at a synchronized equilibrium that yield symmetry-preserving in-phase oscillations, see Fig 2. We calculate the stability of the synchronization manifold near a synchronous equilibrium and combine Hopf criticality results to determine regions of parameter space where the fully synchronized periodic state is asymptotically stable near bifurcation. More importantly, the results are valid for networks of arbitrary size  $N$ . Normal hyperbolicity<sup>22,23</sup> guarantees the synchronization manifold is robust to small non-homogeneities in the STNOs. Numerical simulations show that synchronization is preserved to approximately  $\pm 5\%$  variations in anisotropy strength. Results are illustrated with arrays of up to  $N = 1000$  nano-oscillators, see Fig. 3. The analysis also captures symmetry-breaking patterns of oscillations, but we do not pursue the study of those cases here. These patterns are described as “multiple synchronization attractors” in Li *et al.*<sup>24</sup>.

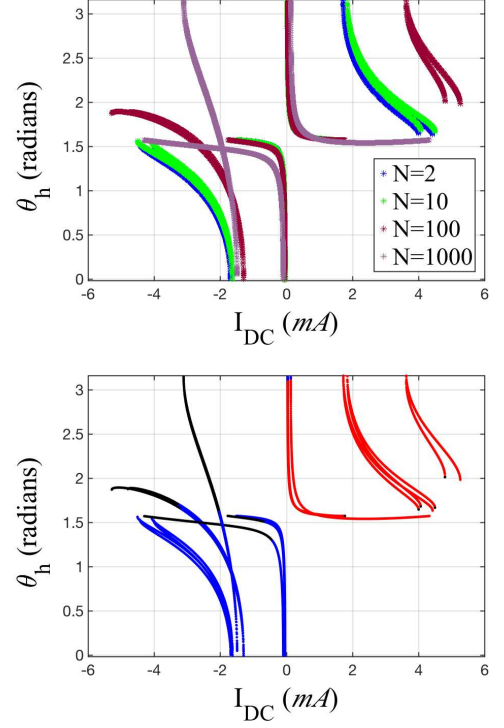


FIG. 2: (Top) Loci of Hopf bifurcations of synchronized oscillations. (Bottom) Stability of synchronization manifold. Red: supercritical Hopf and stable synchronization manifold; black: subcritical Hopf and unstable synchronization manifold; blue: supercritical Hopf and unstable synchronization manifold. The combined results of these two plots reveals the optimal region to synchronize a series array of nano-pillar STNOs: the first quadrant of parameter space  $(I_{DC}, \theta_h)$ . Parameters<sup>25</sup> are:  $N_1 = 1$ ,  $N_2 = 0$ ,  $\gamma = 2.2 \times 10^5 \text{ m} \cdot \text{A}^{-1} \text{ s}^{-1}$ ,  $\alpha = 0.008$ ,  $\kappa = 45 Oe$ ,  $\mu = 0.992$ ,  $h_a = 300 Oe$ ,  $\beta_{\Delta R} = 5.95 \times 10^{-4}$ . (Color online).

## II. LOCI OF STABLE SYNCHRONIZED OSCILLATIONS

The free-layer magnetization vector,  $\hat{m} = [m_1, m_2, m_3]^T$ , for an individual nanopillar oscillator is governed by the Landau-Lifshitz-Gilbert-Slonczewski (LLGS)<sup>26–29</sup> equation

$$\frac{d\hat{m}}{dt} = -\gamma \hat{m} \times \vec{H}_{\text{eff}} + \alpha \hat{m} \times \frac{d\hat{m}}{dt} - \gamma \mu I \hat{m} \times (\hat{m} \times \hat{M}), \quad (1)$$

where  $\gamma$  is the gyromagnetic ratio,  $\alpha$  is the Gilbert damping term,  $\mu$  contains material parameters and  $\vec{H}_{\text{eff}}$  is the effective magnetic field. The term  $\vec{H}_{\text{eff}}$  consists of an anisotropy field,  $\vec{H}_{\text{an}} = \kappa(\hat{m} \cdot \hat{e}_{||})\hat{e}_{||}$ , where  $\kappa$  is the strength of the anisotropy (we set  $\kappa = 45 Oe$  in our simulations<sup>25</sup>) and  $\hat{e}_{||} = [\sin \theta_{||} \cos \phi_{||}, \sin \theta_{||} \sin \phi_{||}, \cos \theta_{||}]^T$  is a preferred direction of magnetization.  $\vec{H}_d$  is a demagnetization field and we set  $\vec{H}_d = -4\pi S_0(N_1 m_1 \hat{x} + N_2 m_2 \hat{y} + N_3 m_3 \hat{z})$  where  $S_0 = 8400/4\pi$  is the constant magnitude

of the average magnetization vector  $S(t)$  (in units of  $Oe$ ) so that  $\hat{m} = S/S_0$ ,  $N_1, N_2, N_3$  are dimensionless constants satisfying  $N_1 + N_2 + N_3 = 1$  and  $\{\hat{x}, \hat{y}, \hat{z}\}$  are the orthonormal unit vectors.  $\vec{H}_{\text{appl}}$  is an applied magnetic field given by  $\vec{H}_{\text{appl}} = h_a [0, \sin \theta_h, \cos \theta_h]^T$ , which we assume to lie on the  $yz$ -plane at some angle  $\theta_h$  instead of the  $z$ -axis, and note that  $h_a$  is in units of  $Oe$ .  $\hat{M}$  is the fixed layer magnetization vector that defines the spin polarization direction of the current. In what follows we assume  $\theta_{||} = 0$  so that  $e_{||} = [0, 0, 1]$ , which produces an easy axis in the  $z$ -direction. Finally, we assume the direction of polarization of the spin-polarized current to remain constant along the  $z$ -direction, i.e.,  $\hat{M} = \hat{z}$ .

For an array of STNOs, coupling occurs if the input current  $I$  is replaced by  $I_j$ . First, we assume the STNOs to be identical. Later, we consider the effects of non-homogeneities as perturbations of the synchronization manifold. Applying Kirchhoff's Laws we obtain the current through the  $j^{\text{th}}$  STNO:

$$I_j = I_{\text{DC}} \left( 1 + \sum_{i=1}^N \beta_{\Delta Ri} \cos \theta_i(t) \right), \quad (2)$$

where  $I_{\text{DC}}$  is a constant DC current,  $\beta_{\Delta Ri}$  is a parameter that depends on the resistances in the parallel and antiparallel magnetization states, and  $\theta_i(t)$  is the angle between the magnetization of the fixed and free ferromagnetic layers. We substitute Eq. (2) into Eq. (1) and, for convenience, we convert to complex stereographic coordinates through the change of variables  $z_j = (m_{j1} + im_{j2})/(1 + m_{j3})$ . Direct calculations yield

$$\begin{aligned} \dot{z}_j = & \frac{\gamma(1 + i\alpha)}{1 + \alpha^2} \left[ ih_{a3}z_j + \frac{h_{a2}}{2}(1 + z_j^2) + i\kappa \frac{1 - |z_j|^2}{1 + |z_j|^2} z_j - \mu I_{\text{DC}} z_j - \right. \\ & \mu I_{\text{DC}} \beta_{\Delta R} \sum_{k=1}^N \frac{1 - |z_k|^2}{1 + |z_k|^2} z_j - \frac{4\pi S_0}{1 + |z_j|^2} \left( \frac{N_1 - N_2}{2} (z_j^3 - \bar{z}_j) + \right. \\ & \left. \left. \left( 1 - \frac{3N_1 + 3N_2}{2} \right) (z_j - z_j |z_j|^2) \right) \right], \quad (3) \end{aligned}$$

where  $h_{a2} = h_a \sin(\theta_h)$  and  $h_{a3} = h_a \cos(\theta_h)$ .

For the special case  $N_1 = N_2 = 0.5$ , Eq. (3) is more amenable to analysis, and thus we can find, via Maple, implicit analytic expressions for the Hopf loci that yield synchronized periodic states for arbitrary arrays of size  $N$ . Although the synchronized periodic oscillation is unstable, we can still use these analytical expressions to follow, via the automatic numerical continuation software AUTO<sup>30</sup>, the movement of the Hopf loci as function of the continuation parameter  $s$ , where  $N_1 = 0.5 + s$  and  $N_2 = 0.5 - s$ . For  $s = 0.5$ , we arrive at the physically-relevant configuration of easy-plane anisotropy or  $x$ -axis demagnetization. The Hopf loci curves for  $s = 0.5$  are shown in Fig. 2 (top) for various sizes of networks. In addition, we determine the criticality of each Hopf loci point through the Lyapunov constant formula<sup>32</sup> as well as the local asymptotic stability of the synchronization manifold near the Hopf point, via AUTO. This process yields, for  $s = 0.5$ , the red Hopf loci curves (color online) located

in the first quadrant of  $(I_{\text{DC}}, \theta_h)$ -space from which stable synchronized periodic solutions bifurcate, see Fig. 2 (bottom).

Observe that the location of these curves implies that less current is required to synchronize larger arrays. This observation suggests that synchronization in series array of nanopillar STNOs depends more on the dynamical parameters than on the coupling strength. Similar results have been observed in studies of power grids, which can also be treated as Kuramoto oscillator networks<sup>31</sup>.

We wish to emphasize that the aim of this manuscript is strictly on the theoretical analysis to determine regions of existence of stable synchronization. Effects of noise, such as linewidth reduction, are briefly addressed in Section VII, but a detailed analysis is ongoing and deferred to a future publication. Next we present an outline of the analysis that was carried out to obtain the implicit solutions of the Hopf loci.

### III. HOPF BIFURCATION CURVES

This section summarizes the mathematical analysis of how one can exploit the symmetry of the network to obtain the main results shown in Fig. 2. Details of these calculations can be found in Appendix A.

Due to the all-to-all coupling that appears in Eq. (3) as a consequence of Kirchhoff's law, and the assumption of identical STNOs, any permutation of the STNOs in the array leaves the coupling term invariant; thus, the series array has symmetry group  $\mathbf{S}_N$ , the group of all permutations of  $N$  objects. To find analytical expressions for the Hopf loci of synchronized solutions we study the linearized system near the origin. Let  $\mathbf{z} = (z_1, \dots, z_N) \in \mathbb{C}^N$  and denote equation (3) by  $\dot{z}_j = f_j(\mathbf{z})$ . Since we assume all the STNO's to be identical, we have  $f_1 = f_2 = \dots = f_N$ . We rewrite the system of Eq. (3) in abbreviated form

$$\dot{\mathbf{z}} = \mathbf{f}(\mathbf{z}), \quad (4)$$

where  $\mathbf{f} = [f_1, \dots, f_N]^T$ . Let  $\mathbf{z}_0 = (z_0, \dots, z_0)$  be an equilibrium solution of (4) with isotropy subgroup  $\mathbf{S}_N$ <sup>21</sup>. Then the linearization at  $\mathbf{z}_0$  is given by

$$\mathbf{L} := \begin{bmatrix} \mathbf{A} & \mathbf{B} & \cdots & \mathbf{B} \\ \mathbf{B} & \ddots & \ddots & \vdots \\ \vdots & \ddots & \ddots & \mathbf{B} \\ \mathbf{B} & \cdots & \mathbf{B} & \mathbf{A} \end{bmatrix} \quad (5)$$

where  $\mathbf{A} = (df_{jj})_{\mathbf{z}=\mathbf{z}_0}$  and  $\mathbf{B} = (df_{jk})_{\mathbf{z}=\mathbf{z}_0}$  are  $2 \times 2$  Jacobian matrices of  $f_j$ , with  $j \neq k$ . Using symmetry methods, we block diagonalize  $\mathbf{L}$  to a form which respects symmetry invariant subspaces. Let  $P$  be the change of coordinates matrix. Applying  $P$  to  $\mathbf{L}$ , we obtain a block diagonalization of the linear part of the coupled STNO

array

$$\tilde{\mathbf{L}} := P^{-1}\mathbf{L}P = \text{diag}\{\mathbf{A} + (N-1)\mathbf{B}, \mathbf{A} - \mathbf{B}, \dots, \mathbf{A} - \mathbf{B}\}. \quad (6)$$

From the diagonal structure, the eigenvalues of the blocks are also eigenvalues of  $\tilde{\mathbf{L}}$ . It follows that Hopf bifurcations in (4) occur if and only if  $\mathbf{A} + (N-1)\mathbf{B}$  or  $\mathbf{A} - \mathbf{B}$  have purely imaginary eigenvalues. In the former case, the eigenspace associated with  $\mathbf{A} + (N-1)\mathbf{B}$  is  $v_0 = [v, \dots, v]^T$  and the symmetry group  $\mathbf{S}_N$  acts trivially on  $v_0$ . This corresponds to a symmetry-preserving Hopf bifurcation in which all STNOs oscillate in synchrony, i.e., same wave form, same amplitude and same phase. In the latter case, the eigenvalues have, generically, multiplicity  $N-1$  (from the  $N-1$  blocks  $\mathbf{A} - \mathbf{B}$ ) and the emerging patterns of oscillations arise via symmetry-breaking Hopf bifurcations<sup>21</sup>. For instance, the case reported in<sup>24</sup>, in which two pairs of STNOs are in-phase with one another and half a period out-of-phase with respect to each pair, corresponds to a Hopf symmetry-breaking pattern that emerges from the  $\mathbf{A} - \mathbf{B}$  block with  $N = 4$ . A complete description of the possible patterns of oscillations that can appear for each value of  $N$  can be found via equivariant Hopf bifurcation<sup>21</sup>. The emphasis of this manuscript is, however, on the symmetry-preserving synchronization state.

Combining the equilibrium conditions with the trace condition of purely imaginary eigenvalues for the block  $\mathbf{A} + (N-1)\mathbf{B}$  and using polar coordinates,  $z_0 = r(\cos \theta + i \sin \theta)$ , we get the following set of equations as a function of  $(r, \cos \theta, I_{DC}, \theta_h)$ :

$$\begin{aligned} \text{Re}(f_j) &= 0 \\ \text{Im}(f_j) &= 0 \\ \text{Tr}(\mathbf{A} + (N-1)\mathbf{B}) &= 0. \end{aligned} \quad (7)$$

To find the desired analytical expressions for the Hopf boundary curves, we solve the first three equations in Eq. (7) implicitly for the state variables  $(r, \theta)$  as functions of the parameters  $I_{DC}$  and  $\theta_h$ . We set  $N_1 = N_2 = 0.5$  as a starting point to facilitate the analysis. Through a series of substitutions we are able to reduce this system of three equations with four unknowns,  $(r, \theta, I_{DC}, \theta_h)$ , to a single expression with two variables  $(r, \theta_h)$ . To plot the boundary curves, we first extract the coordinate points from the solution sets and back-substituting gives the actual point values  $(I_{DC}, \theta_h)$  along the curves. Varying  $N$  we can then trace the movement of the synchronous Hopf bifurcation curves. We verify along the curves obtained that  $\det(\mathbf{A} - \mathbf{B}) > 0$  and  $\det(\mathbf{A} + (N-1)\mathbf{B}) > 0$ . The results just described are then extended using AUTO to the case  $N_1 = 1, N_2 = N_3 = 0$  by continuing the Hopf loci curves in  $(I_{DC}, \theta_h)$  space using  $N_1 = 0.5 + s$  and  $N_2 = 0.5 - s$  and letting the continuation parameter  $s$  evolve from 0 to 0.5.

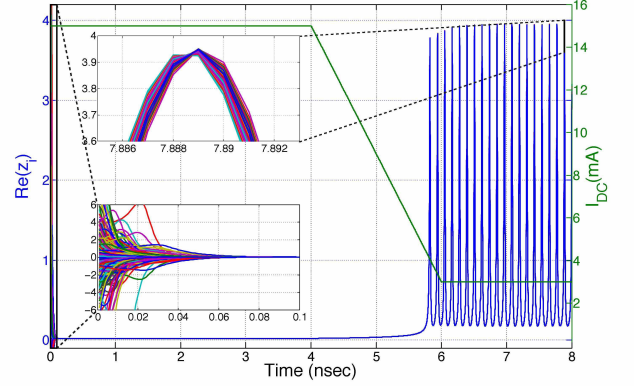


FIG. 3: Locking into synchronization with  $N = 1000$  STNOs. Start at high  $I_{DC}$  and let the system lock into the common equilibrium. Then sweep down  $I_{DC}$  until the common equilibrium vanishes and synchronized oscillations appear. Inset (top): zooms-in on the top part of the oscillation showing a high level of synchronization between all the STNOs. Inset (bottom): zoom-in on the set of random initial conditions for the  $N = 1000$  STNOs and evolution for small time values showing rapid convergence to a synchronized equilibrium.

#### IV. STABILITY

The Hopf bifurcation can be supercritical or subcritical, leading to stable or unstable synchronized oscillations, respectively. Which one appears is determined by the Lyapunov constant<sup>32</sup>. If the Lyapunov constant is negative, the Hopf bifurcation is supercritical while if it is positive, it leads to subcritical Hopf. Now, the stability property of the synchronization manifold is determined by the eigenvalues transverse to the manifold. Those eigenvalues are given by  $N-1$  copies of the eigenvalues of the block  $\mathbf{A} - \mathbf{B}$  and since the synchronization manifold is computed near an equilibrium, then normal hyperbolicity follows from the eigenvalues of the  $\mathbf{A} - \mathbf{B}$  block. The actual calculation of Lyapunov constant and that of the transverse eigenvalues are technical and lengthy and have been moved to Appendix A under nonlinear analysis.

#### V. LOCKING INTO SYNCHRONIZATION

Numerical simulations indicate the common equilibrium state of large arrays has a large basin of attraction for large values of DC current, about 15 mA. This suggests a possible strategy to achieve synchronization in actual experiments: start the experiments at high  $I_{DC}$  current and let the system lock into the common equilibrium. Then sweep down  $I_{DC}$  until the common equilibrium vanishes at a saddle-node bifurcation and stable synchronized oscillations appear, created via Hopf bifurcation from a co-existing common equilibrium found at lower  $I_{DC}$  values. This strategy was tested with



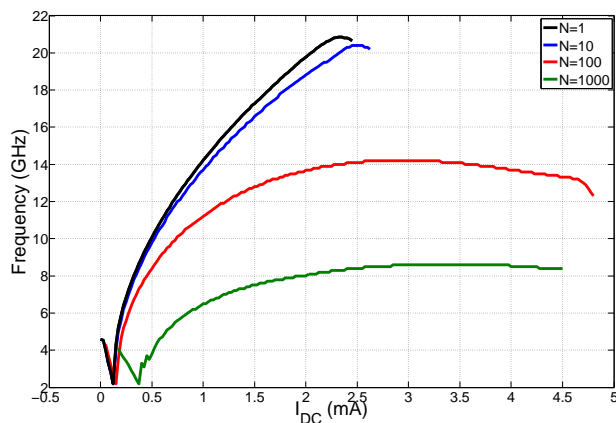


FIG. 4: Frequency response of an array of  $N$  STNOs connected in series. The observed dips in frequency correspond to switching between out-of-plane and in-plane oscillations. Parameters are the same as in Fig. 2, with  $\theta_h = 3\pi/4$ .

non-homogeneities introduced through variations in the anisotropy field constant  $\kappa$ . As a consequence of the normal hyperbolicity of the synchronization manifold, we expect the synchronization state to be robust under small perturbations, such as the non-homogeneities in  $\kappa$ . Indeed, numerical simulations confirm that the STNOs are able to synchronize with up to  $\pm 5\%$  variations in anisotropy strength if the values are chosen randomly from a uniform distribution, see Fig. 3, and up to  $\pm 4\%$  with a Gaussian distribution.

## VI. FREQUENCY RESPONSE

We now employ the Fast Fourier Transform to characterize the frequency response in networks of  $N$  non-identical oscillators coupled in series. The plots in Fig. 4 show the frequency of oscillation for  $N = 1, 10, 100$  and  $1000$ . The observed “dips” for small values of  $I_{DC}$  correspond to the switch from out-of-plane oscillations to in-plane oscillations. For  $\theta_h = 0$ , the switch is characterized by a gluing bifurcation; that is, a global bifurcation where a pair of homoclinic loops (symmetrically related in this case) are connected to a saddle equilibrium, see<sup>34</sup> for an example in the context of STNOs. For  $\theta_h = 3\pi/4$ , which is the value used in Fig. 4, the switch involves two homoclinic bifurcations. In both cases, the switch from out-of-plane to in-plane oscillations explains why the frequency approaches 0 Hz. In general, lines terminating at non-zero frequency correspond to known Hopf bifurcations and lines terminating at or near 0 Hz correspond to suspected (not verified for every value of  $N$ ) homoclinic bifurcations. These results suggest that the range of  $I_{DC}$  values for which oscillations are present increases with the number of STNOs, however the interval of possible frequencies decreases with increased  $N$ .

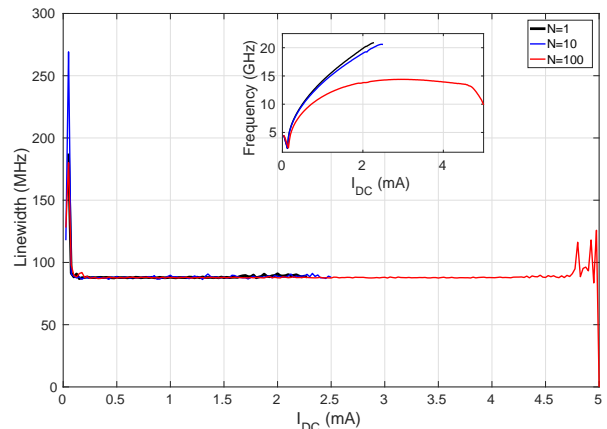


FIG. 5: Linewidth. The observed dips in frequency correspond to switching between out-of-plane and in-plane oscillations. Parameters are the same as in Fig. 2, with  $\theta_h = 3\pi/4$ .

## VII. LINEWIDTH

We now consider (briefly) the effects of thermal noise on the oscillations of the synchronized solutions by adding a stochastic thermal field term  $\vec{H}_{th}$  to  $\vec{H}_{eff}$ <sup>35,36</sup> in the original LLGS Eq. (1), becoming

$$\frac{d\hat{m}}{dt} = -\gamma \hat{m} \times (\vec{H}_{eff} + \vec{H}_{th}) + \alpha \hat{m} \times \frac{d\hat{m}}{dt} - \gamma \mu I \hat{m} \times (\hat{m} \times \hat{M}), \quad (8)$$

where  $\vec{H}_{th} = [h_x(t), h_y(t), h_z(t)]^T$ , in which  $h_x(t)$ ,  $h_y(t)$  and  $h_z(t)$  are Gaussian distributed random functions, uncorrelated, of zero mean. The added term also carries to the complex form Eq. (3). Linewidth was computed as full width of the Power Spectra Decomposition (PSD) of the synchronized oscillations, via FFT, at half maximum of main frequency in the PSD. The computation was carried out as a function of  $I_{DC}$ , on the same interval of the frequency response of Fig 4, and for a few different values of array size  $N$ . The results are shown in Fig. 5.

The spikes in linewidth that are observed near the end points of the interval of synchronization are due to the oscillations having different characteristics. More specifically, for small  $I_{DC}$  the spikes are due to a change to out-of-plane oscillations and for large  $I_{DC}$  (and large arrays) the spikes are due to loss of synchronization, i.e., for large arrays the synchronized oscillations give way to out-of-phase oscillations before eventually converging to an equilibrium point. But for the most part of the interval of synchronization, the linewidth remains relatively small. These results suggest, again, that the synchronized solution is significantly robust against the effects of noise. However, one would have to carry out a complete analysis of the stochastic properties of the coupled network equations as a function of coupling strength and noise inten-

sity, for instance. We also wish to point out that temperature is assumed to be implicitly included in the stochastic thermal field. Future experimental works should provide a more explicit contribution of temperature variations and material properties towards the stochastic field. Those issues are important but they are beyond the scope of the present work. Instead, our emphasis is, mainly, on finding the conditions for the existence and stability of synchronized oscillations in the deterministic system. We expect to carry out the stochastic analysis in future work. In particular, it would be interesting to obtain theoretical formulas (possibly asymptotic for large  $N$ ) for the half-linewidth for serially coupled STNOs using the theory developed in Slavin and Tiberkevich<sup>36</sup>.

## VIII. DISCUSSION AND CONCLUSIONS

To date, the strongest microwave power that has been produced by a single STNO is in the order of  $0.28\mu W$ <sup>33</sup>. As mentioned in the introduction, Grollier *et al.*<sup>1</sup> showed that for an array of  $N = 10$  electrically coupled STNOs, the synchronized array microwave power output increases as  $N^2$ . Thus, if the  $N^2$  law holds in general, 1000 synchronized nano-oscillators, as simulated in this paper, should produce about  $0.28W$ . Communication systems, which require power in the order of milliwatts, e.g., wireless devices, radar, air traffic control, weather forecasting and navigation systems, would only require about 188 nano-oscillators.

In Turtle *et al.*<sup>34</sup>, we showed computationally the nature of the bifurcations leading to these attractors and discovered that changing the angle of the applied magnetization field could enlarge the basin of attraction of the synchronized oscillations. In this work we extended the bifurcation analysis of nanopillar based STNOs connected in series arrays of arbitrary size. We use equivariant bifurcation theory to find the region of existence and stability of the synchronization manifold for which all STNOs oscillate with the same frequency, phase and amplitude. Our approach to achieve synchronization, via non-Adlerian dynamics, employs only the DC current flowing in each STNO and the angle of the applied magnetic field. The main results include implicit solutions of the Hopf loci as a function of the DC current and the applied magnetic field. Normal hyperbolicity of the synchronization manifold implies robustness of the synchronization state to small perturbations, such as those caused by non-homogeneities or imperfections during the manufacturing process. Computer simulations with non-identical STNOs indicate robustness up to  $\pm 5\%$  variations, which is well within typical fabrication processes. It is our hope that the theoretical results and simulations provided in this manuscript will help guide ongoing experiments. The STNOs are currently fabricated using the 50 nano-meter technology where large arrays can be configured on a substrate. Each oscillator is independently isolated and unconnected at the fabrication stage.

Once the devices are finished, the STNOs will be bonded and connected in a series array. The post fabrication bonding and connection will afford us the opportunity to verify the results established in this paper.

## IX. ACKNOWLEDGEMENT

We acknowledge support from ONR Code 30. J.T. and A.P. were supported in part by NSF grant CMMI-1068831. PLB (Discovery Grant) and CD (USRA) acknowledge funding from NSERC Canada.

### Appendix A: Hopf Curves

This Appendix describes the mathematical analysis that was carried out to obtain the boundary curves that lead an array of STNO into and out of synchronization, as is shown in Fig. 2 in the main manuscript. We start by considering again the array dynamics in stereographic coordinates captured by Eq. (3) with the full network in abbreviated form given by Eq. (4).

#### 1. Linear Analysis

Let  $\mathbf{z}_0 = (z_0, \dots, z_0)$  be an equilibrium solution of (4) with isotropy subgroup  $\mathbf{S}_N^{21}$ . Then, as described in the text, the linearization at  $\mathbf{z}_0$  is given by

$$\mathbf{L} := \begin{bmatrix} \mathbf{A} & \mathbf{B} & \cdots & \mathbf{B} \\ \mathbf{B} & \ddots & \ddots & \vdots \\ \vdots & \ddots & \ddots & \mathbf{B} \\ \mathbf{B} & \cdots & \mathbf{B} & \mathbf{A} \end{bmatrix}$$

where  $\mathbf{A} = (df_{jj})_{\mathbf{z}=\mathbf{z}_0}$  and  $\mathbf{B} = (df_{jk})_{\mathbf{z}=\mathbf{z}_0}$  are  $2 \times 2$  Jacobian matrices of  $f_j$ , with  $j \neq k$ . To diagonalize  $\mathbf{L}$ , we employ the  $\mathbf{S}_N$  isotypic decomposition of the phase space  $\mathbb{C}^N$ , which is given by

$$\mathbb{C}^N = V_1 \oplus \mathbb{C}^{N,0},$$

where

$$\begin{aligned} V_1 &= \{(z, \dots, z) | z \in \mathbb{C}\}, \\ \mathbb{C}^{N,0} &= \{(z_1, \dots, z_N) \in \mathbb{C}^N | z_1 + \dots + z_N = 0\} \end{aligned}$$

are absolutely irreducible representations of  $\mathbf{S}_N^{21}$ . Let

$$v_j = [v, \zeta^j v, \zeta^{2j} v, \dots, \zeta^{(N-1)j} v]^T,$$

where  $\zeta = \exp(2\pi i/N)$  and  $v \in \mathbb{R}$ . The vector  $v_0$ , is a basis for  $V_1$  while the remaining vectors  $v_j$ ,  $j = 1, \dots, N-1$ , form a basis for  $\mathbb{C}^{N,0}$ . Now let

$$\begin{aligned} P = [ & \text{Re}\{v_0\}, \text{Im}\{v_0\}, \text{Re}\{\bar{v}_0\}, \text{Im}\{\bar{v}_0\}, \dots, \\ & \text{Re}\{v_{N-1}\}, \text{Im}\{v_{N-1}\}, \text{Re}\{\bar{v}_{N-1}\}, \text{Im}\{\bar{v}_{N-1}\}]^T. \end{aligned}$$

Applying  $P$  to  $\mathbf{L}$ , we obtain the following block diagonalization of the linear part of the coupled STNO array

$$\tilde{\mathbf{L}} := P^{-1}\mathbf{L}P = \text{diag}\{\mathbf{A} + (N-1)\mathbf{B}, \mathbf{A} - \mathbf{B}, \dots, \mathbf{A} - \mathbf{B}\} \quad (\text{A1})$$

From the diagonal structure, the eigenvalues of the blocks are also eigenvalues of  $\tilde{\mathbf{L}}$ . It follows that Hopf bifurcations in (4) occur if and only if  $\mathbf{A} + (N-1)\mathbf{B}$  or  $\mathbf{A} - \mathbf{B}$  have purely imaginary eigenvalues. In the former case, the eigenspace associated with  $\mathbf{A} + (N-1)\mathbf{B}$  is

$$v_0 = [v, \dots, v]^T,$$

where the symmetry group  $\mathbf{S}_N$  acts trivially. This corresponds to a symmetry-preserving Hopf bifurcation in which all STNOs oscillate in synchrony, i.e., same wave form, same amplitude and same phase. In the latter case, the eigenvalues have, generically, multiplicity  $N-1$  (from the  $N-1$  blocks  $\mathbf{A} - \mathbf{B}$ ) and the emerging patterns of oscillations arise via symmetry-breaking Hopf bifurcations<sup>21</sup>. Combining the equilibrium conditions with the trace condition of purely imaginary eigenvalues for the block  $\mathbf{A} + (N-1)\mathbf{B}$  (or equivalently  $\mathbf{A} - \mathbf{B}$  for symmetry-breaking Hopf bifurcation) and using polar coordinates,  $z_0 = r(\cos \theta + i \sin \theta)$ , we get the following set of equations as a function of  $(r, \cos \theta, I_{\text{DC}}, \theta_h)$ :

$$\begin{aligned} \text{Re}(f_j) &= 0 \\ \text{Im}(f_j) &= 0 \\ \text{Tr}(\mathbf{A} + (N-1)\mathbf{B}) &= 0, \end{aligned} \quad (\text{A2})$$

and require

$$\begin{aligned} \text{Tr}(\mathbf{A} - \mathbf{B}) &< 0 \\ \det(\mathbf{A} - \mathbf{B}) &> 0 \\ \det(\mathbf{A} + (N-1)\mathbf{B}) &> 0, \end{aligned}$$

on the solution set of (A2) to guarantee no eigenvalues with positive real parts. To find the desired analytical expressions for the Hopf boundary curves, we solve Eq. (A2) implicitly for the state variables  $(r, \theta)$  as functions of the parameters  $I_{\text{DC}}$  and  $\theta_h$ . We set  $N_1 = N_2 = 0.5$  as a starting point to facilitate analysis. Through a series of substitutions we are able to reduce this system of three equations with four unknowns,  $(r, \theta, I_{\text{DC}}, \theta_h)$ , to a single expression with two variables  $(r, \theta_h)$ . Using Maple's *implicitplot* function 16 times, curves are found in the  $(r, \theta_h)$  domain to account for all possible solutions. Combining results produces the desired zero solution set of Eq. (A2). To plot the Hopf curves, we first extract the coordinate points from the solution sets and back-substituting gives the actual point values  $(I_{\text{DC}}, \theta)$  along the curves. Then we substitute these points to verify that  $\det(\mathbf{A} - \mathbf{B}) > 0$  and  $\det(\mathbf{A} + (N-1)\mathbf{B}) > 0$ . By varying  $N$  in the implicit solver, we are then able to trace the movement of the synchronous Hopf bifurcation curves. As mentioned above, the Hopf curves are extended using AUTO to the case  $N_1 = 1, N_2 = N_3 = 0$  and those are the curves plotted in Fig 2.

## 2. Nonlinear Analysis

We set again  $N_1 = N_2 = 0.5$  as a starting point and assume  $\mathbf{A} + (N-1)\mathbf{B}$  has a pair of purely imaginary eigenvalues and translate the equilibrium  $z_0$  of Eq. (4) to the origin using  $\mathbf{v} = \mathbf{z} - \mathbf{z}_0$ , leading to

$$\dot{\mathbf{v}} = \mathbf{f}(\mathbf{v} + \mathbf{z}_0),$$

where  $f_j$  is given by

$$\begin{aligned} f_j = \frac{\gamma(1+i\alpha)}{1+\alpha^2} & \left[ ih_{a3}(v_j + z_0) + \frac{h_{a2}}{2}(1 + (v_j + z_0)^2) + \right. \\ & i\kappa \frac{1 - |v_j + z_0|^2}{1 + |v_j + z_0|^2} (v_j + z_0) - \mu I_{\text{DC}}(v_j + z_0) - \\ & \mu I_{\text{DC}}\beta_{\Delta R} \sum_{k=1}^N \frac{1 - |v_k + z_0|^2}{1 + |v_k + z_0|^2} (v_j + z_0) + \\ & \left. \frac{2\pi i S_0}{1 + |v_j + z_0|^2} (v_j + z_0 - (v_j + z_0)|v_j + z_0|^2) \right] \quad (\text{A3}) \end{aligned}$$

To determine criticality of the Hopf bifurcation we set  $g(v, \bar{v}) = (1 + |v + z_0|^2)^{-1}$  and Taylor expand Eq. (A3) at  $(0, 0)$  up to cubic order<sup>32</sup>, which yields

$$\dot{v}_j = H_1(v_j, \bar{v}_j, v, \bar{v}) + \mathcal{N}(v_j, \bar{v}_j, v, \bar{v}), \quad (\text{A4})$$

where  $\mathcal{N}(v_j, \bar{v}_j, v, \bar{v}) = H_2(v_j, \bar{v}_j, v, \bar{v}) + H_3(v_j, \bar{v}_j, v, \bar{v})$  with  $H_\ell$  a homogeneous polynomial of degree  $\ell$ . That is,

$$\begin{aligned} H_1(v, \bar{v}) &= a_{10}v_j + a_{01}\bar{v}_j + \sum_{k=1}^n b_{10}v_k + b_{01}\bar{v}_k \\ H_2(v, \bar{v}) &= a_{20}v_j^2 + a_{11}|v_j|^2 + a_{02}\bar{v}_j^2 + \sum_{k=1}^n b_{20}v_k^2 + \\ & b_{11}|v_k|^2 + b_{02}\bar{v}_k + c_{110}v_jv_k + c_{101}v_j\bar{v}_k \\ H_3(v, \bar{v}) &= a_{30}v_j^3 + a_{21}|v_j|^2v_j + a_{12}|v_j|^2\bar{v}_j + a_{03}\bar{v}_j^3 + \\ & \sum_{k=1}^n b_{30}v_k^3 + b_{21}|v_k|^2v_k + b_{12}|v_k|^2\bar{v}_k + b_{03}\bar{v}_k^3 + \\ & (c_{120}v_k^2 + c_{111}|v_k|^2 + c_{102}\bar{v}_k^2)v_j. \end{aligned}$$

For brevity, we list only a few of the coefficients:

$$\begin{aligned} b_{10} \tau &= \mu I_{\text{DC}}\beta_{\Delta R}(2g(0, 0)^2|z_0|^2) \\ a_{10} \tau &= ih_{a3} + z_0h_{a2} + i\kappa g(0, 0)^2(1 - 2|z_0|^2 - |z_0|^4) - \mu I_{\text{DC}} - \\ & \mu I_{\text{DC}}\beta_{\Delta R}g(0, 0)^2(N(1 - |z_0|^4) - 2|z_0|^2) + \\ & 2\pi i S_0 g(0, 0)^2(1 - 2|z_0|^2 - |z_0|^4) - b_{10} \tau \\ b_{11} \tau &= -2\mu I_{\text{DC}}\beta_{\Delta R}z_0(|z_0|^2 - 1)g(0, 0)^3 \\ c_{101} \tau &= 2\mu I_{\text{DC}}\beta_{\Delta R}z_0g(0, 0)^2 \\ a_{11} \tau &= -4z_0g(0, 0)^3(i\kappa + \frac{i}{2} - \mu I_{\text{DC}}\beta_{\Delta R}) - b_{11} \tau - c_{101} \tau, \end{aligned}$$

where  $\tau = (1 + \alpha^2)/(\gamma(1 + i\alpha))$ .

We now rewrite Eq. (A4) using the same matrix  $P$  given by the decomposition of  $\mathbb{C}^N = \mathbb{C}^{N,0} \oplus V_1$  into  $\mathbf{S}_N$  irreducible representations and letting  $v = Pu$  yields

$$\dot{u} = \tilde{\mathbf{L}}u + P^T\mathbf{N}(Pu, \bar{Pu}),$$

where  $\tilde{\mathbf{L}} = P^T\mathbf{L}P$  are the linear terms given by Eq. (A1) and the nonlinear terms are  $\mathbf{N}(v, \bar{v}) = (\mathcal{N}(v_1, \bar{v}_1, v, \bar{v}), \dots, \mathcal{N}(v_N, \bar{v}_N, v, \bar{v}))^T$ .



An important observation is that the center manifold is  $V_1 = \text{Fix}(\mathbf{S}_N)$  and so the flow-invariant center manifold is in fact a subspace for Eq 4. Thus we can compute the criticality of the Hopf bifurcation directly from the equation for  $\dot{u}_1$  evaluated at  $u_\ell = \bar{u}_\ell = 0$  for  $\ell = 2, \dots, N$ , which yields

$$\begin{aligned} \dot{u}_1 = & G_{10}u_1 + G_{01}\bar{u}_1 + G_{20}u_1^2 + G_{11}|u_1|^2 + G_{02}\bar{u}_1^2 + \\ & G_{30}u_1^3 + G_{21}|u_1|^2u_1 + G_{12}|u_1|^2\bar{u}_1 + G_{03}\bar{u}_1^3, \end{aligned} \quad (\text{A5})$$

where

$$\begin{aligned} G_{10} &= a_{10} + Nb_{10} \\ G_{01} &= a_{01} + Nb_{01} \\ G_{20} &= (a_{20} + N(b_{20} + c_{110}))/\sqrt{N} \\ G_{11} &= (a_{11} + N(b_{11} + c_{101}))/\sqrt{N} \\ G_{02} &= (a_{02} + Nb_{02})/\sqrt{N} \\ G_{30} &= (a_{30} + \sqrt{N}(b_{30} + c_{120}))/\sqrt{N} \\ G_{21} &= (a_{21} + \sqrt{N}(b_{21} + c_{111}))/\sqrt{N} \\ G_{12} &= (a_{12} + \sqrt{N}(b_{12} + c_{102}))/\sqrt{N} \\ G_{03} &= (a_{03} + \sqrt{N}b_{03})/\sqrt{N}. \end{aligned}$$

Now, at a Hopf bifurcation,  $\text{Re}(G_{10}) = 0$  and the eigenvalues are  $\pm i\rho$  with

$$\rho := \sqrt{|G_{10}|^2 - |G_{01}|^2}.$$

We use the linear transformation

$$Q = \begin{pmatrix} G_{01} & i\text{Im}(G_{10}) - i\rho \\ -i\text{Im}(G_{10}) + i\rho & \bar{G}_{01} \end{pmatrix}$$

and the change of coordinates  $[w_1, \bar{w}_1] = Q[u_1, \bar{u}_1]^T$  to diagonalize the linear part of Eq. (A5) to  $\text{diag}(i\rho, -i\rho)$ . Let  $\tilde{H}_\ell(w_1, \bar{w}_1) = Q^{-1}H_\ell(Q(w_1, \bar{w}_1)^T)$  for  $\ell = 2, 3$ , then

$$\begin{aligned} \dot{w}_1 = & i\rho w_1 + \frac{\rho + \text{Im}(G_{10})}{2G_{01}\rho} \left( \tilde{H}_2(w_1, \bar{w}_1) + \tilde{H}_3(w_1, \bar{w}_1) \right) \\ & - \frac{i}{2\rho} \left( \overline{\tilde{H}_2(w_1, \bar{w}_1)} + \overline{\tilde{H}_3(w_1, \bar{w}_1)} \right). \end{aligned} \quad (\text{A6})$$

We denote by  $g_{ij}$  the coefficients of the quadratic and cubic terms;  $i + j = \ell$  and  $\ell = 2, 3$ . For the quadratic terms, the coefficients are:

$$\begin{aligned} g_{20} &= \frac{(\rho + \text{Im}(G_{10}))}{2G_{01}\rho} (4G_{20}G_{01}^2 + G_{11}(-2G_{10}G_{01}i + 2iG_{01}\rho) + \\ & G_{02}(-G_{10}^2 + 2G_{10}\rho - \rho^2)) - \\ & \frac{i}{2\rho} \left( \overline{4G_{20}G_{01}^2 + G_{11}(-2G_{10}G_{01}i + 2iG_{01}\rho) +} \right. \\ & \left. \overline{G_{02}(-G_{10}^2 + 2G_{10}\rho - \rho^2)} \right) \\ g_{11} &= \frac{(\rho + \text{Im}(G_{10}))}{2G_{01}\rho} (8G_{20}G_{01}^2 + G_{11}(-4G_{10}G_{01}i) + \\ & G_{02}(-2G_{10}^2 + 2\rho^2)) - \\ & \frac{i}{2\rho} \left( \overline{8G_{20}G_{01}^2 + G_{11}(-4G_{10}G_{01}i) +} \right. \\ & \left. \overline{G_{02}(-2G_{10}^2 + 2\rho^2)} \right) \\ g_{02} &= \frac{(\rho + \text{Im}(G_{10}))}{2G_{01}\rho} (4G_{20}G_{01}^2 + G_{11}(-2G_{10}G_{01}i - 2iG_{01}\rho) + \\ & G_{02}(-G_{10}^2 - 2G_{10}\rho - \rho^2)) - \\ & \frac{i}{2\rho} \left( \overline{4G_{20}G_{01}^2 + G_{11}(-2G_{10}G_{01}i - 2iG_{01}\rho) +} \right. \\ & \left. \overline{G_{02}(-G_{10}^2 - 2G_{10}\rho - \rho^2)} \right), \end{aligned}$$

and the cubic coefficient is:

$$g_{21} = \frac{(\rho + \text{Im}(G_{10}))}{2G_{01}\rho} W - \frac{i}{2\rho} \bar{W}.$$

where

$$\begin{aligned} W := & (12G_{30}G_{01}^3 + G_{21}(-6G_{10}G_{01}^2i + 2iG_{01}^2\rho) \\ & + G_{12}(4G_{10}G_{01}(-G_{10} + \rho) - 2G_{10}(G_{10} - \rho)) \\ & + 2G_{01}\rho(G_{10} + \rho) + G_{03}((G_{10}^2 - 2G_{10}\rho + \rho^2)(G_{10} + \rho)i \\ & + 2i(\rho^2 - G_{10}^2)(-G_{10} + \rho))) \end{aligned}$$

### 3. Lyapunov Constant and Stability

Using the coefficients just listed above, we then obtain the Lyapunov constant from the formula<sup>32</sup>

$$\text{Re}(c_1) = \text{Re} \left( \frac{i}{2\rho} \left( g_{20}g_{11} - 2|g_{11}|^2 - \frac{1}{3}|g_{02}|^2 \right) + \frac{g_{21}}{2} \right). \quad (\text{A7})$$

The Hopf bifurcation is supercritical if  $\text{Re}(c_1) < 0$  and subcritical if  $\text{Re}(c_1) > 0$ . However, this condition only determines the stability of the synchronized periodic solution on the center manifold. Thus, we also need to consider the eigenvalues transverse to the center manifold. Those eigenvalues are given by  $N - 1$  copies of the eigenvalues of the block  $\mathbf{A} - \mathbf{B}$  with real parts  $\frac{1}{2} \text{Tr}(\mathbf{A} - \mathbf{B}) = \text{Re}(a_{10} - b_{10})$ . It follows that the synchronized oscillations are asymptotically stable if  $\text{Re}(a_{10} - b_{10}) < 0$ .

For  $N_1 = N_2 = 0.5$ , subcritical Hopf bifurcations are obtained. We change the direction of demagnetization to  $N_1 = 1$ ,  $N_2 = N_3 = 0$  by numerical continuation using AUTO and we obtain that, Hopf bifurcation curves in the first quadrant of  $(I_{\text{DC}}, \theta_h)$  space are supercritical and the synchronization manifold is asymptotically stable near  $z_0$ . This leads to an asymptotically stable periodic solution near bifurcation. See Fig 2.

- 
- \* Electronic address: jturtle6294@yahoo.com  
† Electronic address: Pietro-Luciano.Buono@uoit.ca  
‡ Electronic address: palacios@euler.sdsu.edu  
§ Electronic address: christinedabrowski15@gmail.com  
¶ Electronic address: visarath@spawar.navy.mil  
\*\* Electronic address: patrick.longhini@navy.mil
- <sup>1</sup> J. Grollier, V. Cros and A. Fert. *Phys. Rev. B, Rapid Comm.* **73**, 060409 (2006).
  - <sup>2</sup> S. Kaka, M.R. Pufall, W.H. Rippard, T.J. Silva, S.E. Russek, and J.A. Katine. *Nature Lett.* **437**, no. 15, 389–392 (2005).
  - <sup>3</sup> J. Persson, Y. Zhou and J. Akerman. *J. of Appl. Physics* **101**, 09A503 (2007).
  - <sup>4</sup> R. Adler. *Proc. IEEE* **61**, 1380–1385 (1973).
  - <sup>5</sup> Z. Li, Y.C. Li and S. Zhang. *Phys. Rev. B* **74**, 054417 (2006).
  - <sup>6</sup> B. Georges, J. Grollier, M. Darques, V. Cros, C. Deranlot, B. Marcilhac, G. Faini and A. Fert. *Phys. Phys. Lett.* **101**, 017201 (2008).
  - <sup>7</sup> V. Tiberkevich, A. Slavin, E. Bankowski and G. Gerhart. *Appl. Phys. Lett.* **95**, 262505 (2009).
  - <sup>8</sup> S. Urazhdin, P. Tabor, V. Tiberkevich and A. Slavin. *Phys. Rev. Lett.* **105**, 104101 (2010).
  - <sup>9</sup> B. Subash, V.K. Chandrasekar and M. Lakshmanan. *EuroPhys. Lett.* **109**, 170009 (2015).
  - <sup>10</sup> A. Houshang, E. Iacocca, P. Durrenfeld, S.R. Sani, J. Akerman and R.K. Dumas. *Nature Nanotechnology* **11**, 280–286 (2016).
  - <sup>11</sup> T. Kendziorczyk, S.O. Demokritov and T. Kuhn. *Phys. Rev. B* **90**, 054414 (2014).
  - <sup>12</sup> B. Georges, J. Grollier, V. Cros and A. Fert. *Appl. Phys. Lett.* **92**, 232504 (2008).
  - <sup>13</sup> Y. Kuramoto. in *Proceedings of the International Symposium on Mathematical Problems in Theoretical Physics*, edited by H. Araki, Lecture Notes in Physics (Springer, Berlin 1975), Vol. 39.
  - <sup>14</sup> A. Slavin and V. Tiberkevich. *IEEE Transactions on Magnetics*, **45:4**, 1875–1918 (2009).
  - <sup>15</sup> E. Iacocca and J. Akerman. *J. of Appl. Physics* **110**, 103910 (2011).
  - <sup>16</sup> M.G. Rosenblum, A.S. Pikovsky and J. Kurths. *Phys. Rev. Lett.* **78**, 4193–1–4 (1997).
  - <sup>17</sup> Z. Zeng, G. Finocchio and H. Jiang. *Nanoscale* **5**, 2219–2231 (2013).
  - <sup>18</sup> L.V. Gambuzza, J. Gomez-Gardenes and M. Frasca. *Sci Rep* **6**, 24915 (2016).
  - <sup>19</sup> F. B. Mancoff, N. D. Rizzo, B. N. Engel and S. Tehrani. *Nature Lett.* **437**, no. 15, 393–395 (2005).
  - <sup>20</sup> D. Li, Y. Zhou, C. Zhou and B. Hu. *Phys. Rev. B* **82**, 140407 (2010).
  - <sup>21</sup> M. Golubitsky, I. N. Stewart, and D. G. Schaeffer. *Singularities and Groups in Bifurcation Theory Vol. II*, vol. 69. Springer-Verlag, New York, 2004.
  - <sup>22</sup> N. Fenichel. *Indiana University Math. J.* **21**, no. 3, 193–226 (1971).
  - <sup>23</sup> M.W. Hirsch, C.C. Pugh and M. Shub. *Invariant Manifolds*, Lecture Notes in Physics (Springer-Verlag, New York 1977), Vol. 583.
  - <sup>24</sup> D. Li, Y. Zhou, B. Hu, J. Akerman and C. Zhou. *Phys. Rev. B* **86**, 014418 (2012).
  - <sup>25</sup> S. Muruges and M. Lakshmanan. *Chaos, Solitons and Fractals* **41**, 2773–2781 (2009).
  - <sup>26</sup> L. Berger. *Phys. Rev. B* **54**, no. 13, 9353–9358 (1996).
  - <sup>27</sup> M. Lakshmanan and K. Nakamura. *Phys. Rev. Letters* **53**, no. 26, 2497–2499 (1984).
  - <sup>28</sup> M. Lakshmanan. *Phil. Trans. R. Soc.* **369**, 1280–1300 (2011).
  - <sup>29</sup> C.S. Liu, K.C. Chen, and C.S. Yeh. *J. of Marine Sci. and Tech.* **17**, no. 3, 228–237 (2009).
  - <sup>30</sup> E. Doedel and X. Wang. *Auto94: Software for Continuation and Bifurcation Problems in Ordinary Differential Equations*, Applied Mathematics Report, California Institute of Technology, July 1994.
  - <sup>31</sup> P.S. Skardal and A. Arenas. *Sci. Adv.* **1**, no. 7, e1500339 (2015).
  - <sup>32</sup> Y. Kuznetsov. *Elements of Applied Bifurcation Theory*. Springer-Verlag, New York, 1988.
  - <sup>33</sup> Z. Zeng and P.K. Amiri and I.N. Krivorotov and H. Zhao and G. Finocchio and J.P. Wang and J.A. Katine and Y. Huai and J. Langer and K. Galatsis and K.L. Wang and H.W. Jiang. *ACS Nano* **6**, no. 7, 6115–6121 (2012).
  - <sup>34</sup> J. Turtle, K. Beauvais, R. Shaffer, A. Palacios, V. In, T. Emery and P. Longhini *J. of Appl. Physics* **113**, 114901 (2013).
  - <sup>35</sup> H.Q. Cui, L. Cai, L. Ni, P. Wei, C.W. Feng and X.K. Yang *J. Supercond. Nov. Magn.* **29**, 2873–2879 (2016).
  - <sup>36</sup> A. Slavin and V. Tiberkevich. *IEEE Transactions on Magnetics* **45**, no. 4, 1875–1918 (2009).